Environ Fluid Mech
DOI 10.1007/s10652-016-9459-y

ORIGINAL ARTICLE

Scale dependency of dynamic relative permeability–satuartion curves in relation with fluid viscosity and dynamic capillary pressure effect

Gaurav Goel[1] · Luqman K. Abidoye[2] · Bhagu R. Chahar[3] · Diganta B. Das[2]

Received: 11 October 2014 / Accepted: 4 May 2016

Abstract Capillary pressure–saturation-relative permeability relationships (P_c–S_w–K_r) are functions of importance in modeling and simulations of the hydrodynamics of two-phase flow in porous media. These relationships are found to be affected by porous medium and fluid properties but the manner in which they are affected is a topic of intense discussion. For example, reported trends in fluid viscosity and boundary conditions effects have been found to be contrary to each other in different studies. In this work, we determine the dependency of dynamic K_r–S_w relationships (averaged data) on domain scale in addition to investigating the effects of fluid viscosity and boundary pressure using silicone oil (i.e. 200 and 1000 cSt) and water as the respective non-wetting and wetting fluids with a view to eliminating some of the uncertainties reported in the literature. Water relative permeability, K_{rw}, was found to increase with increasing wetting phase saturation but decreases with the increase in viscosity ratio. On the other hand, the oil relative permeability, K_{rnw}, was found to increase with the increasing non-wetting phase saturation in addition to the increase in viscosity ratio. Also, it was found that with the increasing boundary pressure K_{rw} decreases while K_{rnw} increases. The influence of scale on relative permeability was slightly indicated in the non-wetting phase with K_{rnw} decreasing as domain size increases. Effect of measurement location on dynamic relative permeability was explored which is rarely found in the literature. Comparison was also made between K_r–S_w relationships obtained under static and dynamic condition. Finally, mobility ratio (m) and dynamic coefficient (τ) were plotted as a function of water saturation (S_w), which showed that m decreases as τ increases at a given saturation, or vice versa.

Keywords Capillary pressure · Relative permeability · Saturation · Two-phase flow · Porous media · Upscaling · Dynamic capillary pressure effect

✉ Diganta B. Das
D.B.Das@lboro.ac.uk

[1] Department of Civil Engineering, Indian Institute of Technology (IIT), Guwahati, Assam, India

[2] Department of Chemical Engineering, Loughborough University, Loughborough, UK

[3] Department of Civil Engineering, Indian Institute of Technology Delhi, New Delhi, India

Published online: 10 May 2016

1 Introduction

The capillary pressure–saturation-relative permeability (P_c–S_w–K_r) relationships for two-phase flow in porous media have been extensively investigated as function of porous media, fluid properties and flow conditions. Such studies are conducted in order to fully define the hydrodynamic behaviour of a number of engineering problems, e.g., immiscible contaminants remediation. Relative permeability-saturation (K_r–S_w) and capillary pressure–saturation (P_c–S_w) relationships are used to describe the complex interplay of capillary, gravitational and viscous forces which affect the two-phase flow in porous media [1]. But, the non-uniqueness in these relationships is well acknowledged. For example, for the P_c–S_w relationships and their saturation-rate dependency, depend on factors such as fluid properties like viscosity and density ratios [2–5], domain scale [6–9], media permeability [7, 10, 11], micro-heterogeneities [9, 12], and hysteresis in P_c–S_w relationships [9], among others. Hou et al. [13] explored the influence of measurement sensor's response on the magnitude of the dynamic capillary effects at scale of a representative elementary volume (REV) and argue that the effects may be due to the experimental measurement artifacts. Their acknowledgement of the impact of the micro-heterogeneities on the dynamic capillary effects, at larger scales, is in agreement with the earlier submission of Das et al. [12] and Mirzaei and Das [14].

This saturation-rate dependency of the system properties observed during non-steady state two-phase flow is referred to as dynamic capillary pressure effects [15] and a large body of literature involving experimental, modeling and theoretical studies has emerged concerning these phenomena [3, 4, 7, 13, 15–25]. Studies by Stauffer [23], Kalaydjian [18], Hassanizadeh and Gray [26] suggest that an extension of the P_c–S_w function should include a saturation rate dependent term. This modification is expressed as:

$$\mathrm{P_c^{dyn}} = P_n^{dyn} - P_w^{dyn} = \mathrm{P_c^{static}} - \tau\left(\frac{\partial \mathrm{S_w}}{\partial \mathrm{t}}\right) \tag{1}$$

where $\mathrm{P_c^{dyn}}$ (kg m^{-1} s^{-2}) is the phase pressure difference measured under dynamic or non-equilibrium conditions, P_n^{dyn} (kg m^{-1} s^{-2}) is the non-wetting phase pressure, P_w^{dyn} (kg m^{-1} s^{-2}) is the wetting phase pressure, $\mathrm{P_c^{static}}$ (kg m^{-1} s^{-2}) is the capillary pressure measured under static or equilibrium conditions, $\frac{\partial \mathrm{S_w}}{\partial \mathrm{t}}$ (s^{-1}) is the desaturation rate, and τ (kg m^{-1} s^{-1}) is called dynamic coefficient.

Determining the P_c–S_w and K_r–S_w relationships experimentally for both the quasi-static and dynamic conditions in the laboratory is time consuming and researchers often resort to indirect estimation of the K_r–S_w relationship using the P_c–S_w curve with the aid of the relative permeability models like the ones in Burdine [27] and Mualem [28]. These are most frequently used to simulate two-phase flow though there exist other categories of K_r–S_w constitutive models, e.g., empirical and analogy based models [29]. By estimating the K_r–S_w relationships from experimental P_c–S_w curves, the transfer of above-mentioned inherent non-uniqueness in the P_c–S_w relationships becomes inevitable. Corroborating this assertion, Gao et al. [30] observed that dynamic effects on relative permeability become more important as the pore size increases. Thus, investigating the relationships of the K_r–S_w curve with some of the above-mentioned factors including the dynamic capillary pressure effects is an effort in the right direction.

Even though some of the factors above were reported to have influences on the K_r–S_w relationships, the consistencies of the trend cannot be affirmed. For example, the reported effects of viscosity on K_r–S_w relationships in the literature have been inconsistent [31–41].

Few experimental studies [32, 38] show that relative permeability decreases with increasing viscosity ratio, $\left(\frac{\mu^n}{\mu^w}\right)$, where μ^n and μ^w are the viscosities of the non-wetting and wetting phases, respectively. Another experimental study [33] shows that both oil (non-wetting) and water (wetting) relative permeability increase with increasing viscosity ratio. On the other hand, numerical and modeling studies [31, 35, 41] demonstrate that water relative permeability decreases while oil relative permeability increases with increasing viscosity ratio. These are obvious inconsistencies, which warrant further investigations.

Also, the porous medium property effects on the relative permeability had been shown to be significant. Das et al. [12] investigated the effects of grain size, amount and distribution of micro-heterogeneities on the K_r–S_w relationship and found that water relative permeability was higher in coarse grain sand, while oil relative permeability was higher in fine grain sand. The effects of gravity were neglected in earlier work [42] but these were included in the latter work [12]. They [12] further showed that larger intensity of heterogeneity led to higher irreducible water saturation in addition to having significant effect on K_r–S_w relationship. Petersen et al. [43] mentioned the significance of pore geometry and flow behaviour on K_r–S_w relationship. Recently, Dou and Zhou [35] reported that in case of large capillary number $\left(\mathrm{Ca} = \frac{\mu u}{\gamma}\right)$ presence of heterogeneity would result in a decrease of oil relative permeability while it would be opposite in case of homogeneous media.

As discussed earlier, many recent studies have observed a non-uniqueness of P_c–S_w curves in terms of dynamic effects in capillary pressure. For example, the experimental results by Goel and O'Carroll [3] and Das and Mirzaei [44] on dynamic capillary pressure effects, namely the dynamic coefficient-saturation (τ–S_w) relationships, provide some highlights on these factors as shown in Fig. 1. Both of the studies were conducted for primary drainage (PD) under quasi-static and dynamic conditions, i.e., in the cases when $\partial S_w/\partial t$ values are near and far from zero, respectively. Goel and O'Carroll [3] used F70 silica sand as porous media having a mean permeability of 1.42×10^{-11} m^2. Water and silicone oil with two differing viscosities (i.e. 0.65 and 5 cSt) were used as the respective wetting and non-wetting fluids. Pressures of both phases and water saturation were measured using tensiometers and EC-5 probes at three levels inside the domain. Das and Mirzaei [44] used two different sands with mean permeabilities of 8.7×10^{-10} m^2 and 3.1×10^{-10} m^2 along with water and silicone oil of viscosity 200 cSt which is higher than what [3] used. The results obtained in the two studies are different owing to not only porous medium properties (e.g., permeability, particle size) and fluid properties but also the domain size. While the domain in one study [3] was a cylindrical column 20 cm long and 10 cm inner diameter, in the other study [44] it was cylindrical column 12 cm long and 10.2 cm inner diameter. Therefore, we can understand that domain size is an important factor influencing dynamic effects in capillary pressure. It also implies that these factors must have profound impact on the dynamic K_r–S_w relationship.

It is indeed a matter of great interest how the dynamic K_r–S_w relationship will be affected by porous medium properties, fluid viscosity and domain size. This is because different pressure gradients and saturation distributions are created in the domain as the viscosity of the fluids, porous medium permeability and domain size change which also affect the dynamic coefficient. Joekar-Niasar and Hassanizadeh [5] explained that τ (Eq. 1) depends on both the viscosity ratio as well as an effective viscosity which rely on the fluid viscosities of the wetting and non-wetting phases. The authors argue that if the viscosity ratio is less than one under drainage, the invading front can become unstable. Such

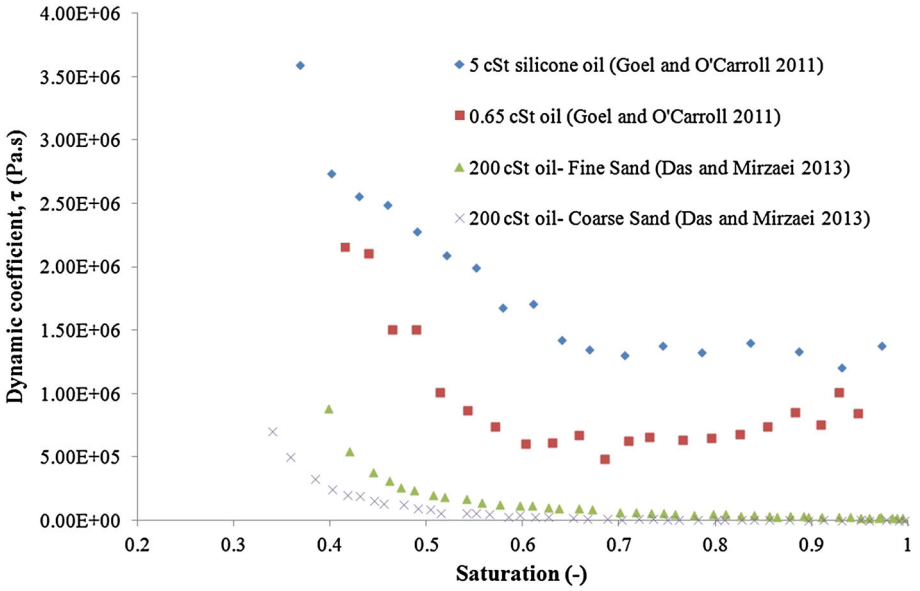

Fig. 1 Comparison of dynamic coefficient—water saturation curves for water and silicone oil with three differing silicone viscosities (0.65, 5 and 200 cSt respectively). Data for silicone oil with 0.65 and 5 cSt are taken from Goel and O'Carroll [3] and remaining data for 200 cSt are from Das and Mirzaei [44]. Goel and O'Carroll [3] used sand having a mean permeability of 1.42×10^{-11} m^2. Das and Mirzaei [44] used two different sands with mean permeabilities of 8.7×10^{-10} m^2 (coarse sand) and 3.1×10^{-10} m^2 (fine sand)

instability of fluid/fluid interfaces leading to the formation of fingers have also been observed by a number of other authors (e.g. [45, 46]). The appearances and disappearances of instabilities and overshoots during two-phase flow in porous media are shown theoretically by means of travelling wave analysis by van Duijn et al. [47]. Fingering is also discussed in detail by Rohde and Kissling [48], Kissling et al. [49] and DiCarlo [50]. As the dynamic saturation front in a porous domain could vary within the domain and K_r relationships are primarily point relationships, it becomes important to know the location dependent K_r–S_w relationship. When the K_r data are averaged over a domain, the average K_r data are likely to be different from the location dependent K_r data because the K_r–S_w relationships are non-linear relationships. However, the significance of this difference is not very well understood for dynamic two-phase flow conditions. Finally, there is little known about the relationships between the dynamic relative permeability and dynamic capillary pressure effects.

Indeed the scale dependency and methods for upscaling of P_c–S_w, K_r–S_w and τ–S_w relationships had been the subjects of intense study in the literature [7, 51–56]. Barker and Thibeau [51] and Renard and De Marsily [54] suggested that the constitutive relationship should be used at the same scale as that of a predictive model but the practicality would only be attained with upscaling. In this regard, Gasda and Celia [52] proposed correction for the coarse grid simulation so that it could match better with the fine grid simulations. Just like the P_c–S_w relationships, Sharifi and Kelkar [55] showed that upscaled relative permeability was time dependent and large scale constitutive relationships were mainly controlled by permeability variation of the porous media [56].

The above discussions present the factors that affect the properties of the two-phase system. We further explained the inconsistencies in reports regarding the trends of the effects of these factors on K_r–S_w relationships. However, we are confronted with the obvious challenge of identifying the true situation of these relationships with regards to the scale of the domain. In particular, we believe there is little discussion on the scale dependency of the dynamic relative permeability-saturation (K_r–S_w) curves in relation to τ–S_w relationships in the open literature. In this work, we intend to determine the effects of scale and fluid properties on K_r–S_w relationships in order to ascertain the trend that exists between them. We use high values viscosity ratios (200 and 1000) in contrast to most previous studies so that the ambiguity in this relationship can be understood further. To avoid the influence of intra-domain averaging technique as employed in most of the literature reports, we use separate and different domain sizes (8 and 12 cm high cylindrical cells) as experimental domains. The effects of boundary pressures and measurement locations within the domain in relation to the domain boundary on the results are determined.

2 Materials and methods

2.1 Porous medium, domain size and fluid properties

All experiments to determine capillary pressure–saturation relationships were conducted in two different cylindrical columns where the first column has dimensions of 8 cm height by 10.2 cm diameter while the second column has dimensions of 12 cm height by 10.2 cm diameter. Henceforth, we shall refer to the former as 8 cm domain and the latter as 12 cm domain. Details are shown in the experimental set up diagram (Fig. 2). The sand used as porous medium was obtained from commercial samples (Minerals Marketing Company, Cheshire, UK) with mean particle diameter of 482 μm. Details of the medium and fluids properties are shown in Table 1. Fluid pairs used were deionised water and silicone oil. Silicone oils with two distinctly different viscosities (200 and 1000 cSt respectively) (Basildon Chemicals, Abingdon, UK) were used. Dynamic experiments were conducted with two different oil injection pressures (Dirichlet boundary condition) at the top boundary of the domain. They were 10 and 20 kPa.

2.2 Instrumentation and column preparation

Based on the domain size, pressure transducers (PTs) (WIKA Instruments Ltd, Redhill, UK), were positioned at different levels of the domain. Two pairs of PTs were attached to the 8 cm high cell at distances of 2 and 6 cm respectively from top boundary (injection point). These pairs were referred to as top and bottom measurement points, respectively. For 12 cm high cell, three pairs of PTs were attached at distances 2, 6 and 10 cm respectively. They were also referred to as top, middle and bottom measurement points respectively. In each pair, one PT was configured to measure silicone oil phase (hydrophobic) while the other measured water phase (hydrophilic) pressure. To achieve this, hydrophilic nylon (pore size: 0.1 μm) and hydrophobic polytetrafluoroethylene, PTFE (pore size: 1 μm) membranes (Porvair Filtration Group Ltd, Hampshire, UK) were used on the respective faces of the PTs. These thin membranes were supported by Vyon filters approximately 5 mm thick (Porvair Filtration Group Ltd, Hampshire, UK). For every pair

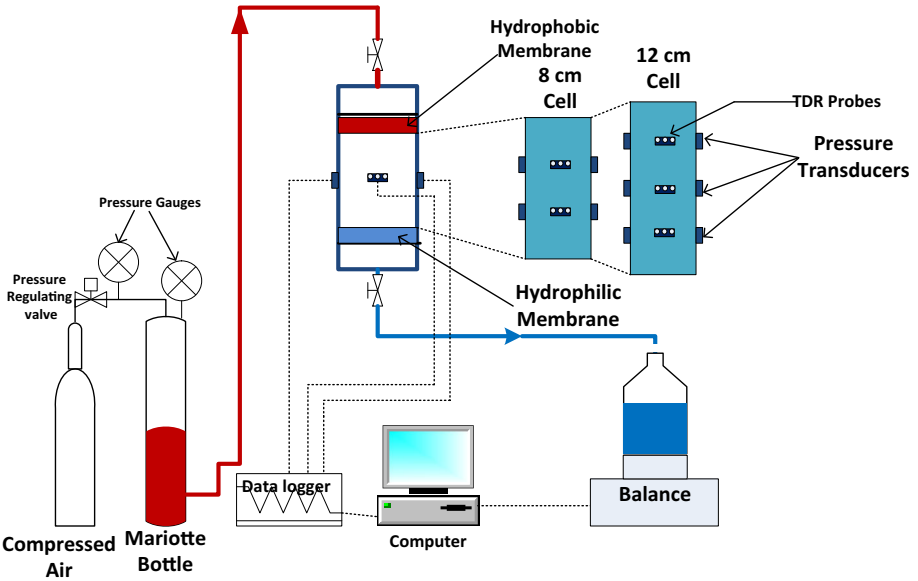

Fig. 2 Diagram of experimental set up showing the two core scale domains (i.e., 8 and 12 cm) used in this work (adopted from [57])

Table 1 Fluid and material properties

Properties	Porous material	Silicone oil		Water
		1	2	
Permeability, K (m^2)	5.66×10^{-11}[a]	–	–	–
Porosity, ϕ (–)	0.37	–	–	–
Particle density (g/cm^3)	2.66	–	–	–
Average particle diameter, D_p (μm)	482.4	–	–	–
Particle size range (μm)	$100 < D_p < 900$	–	–	–
Viscosity, μ (cSt)	–	200[b]	1000[b]	1[c]
Specific gravity, 25 °C	–	0.972	0.974	1
Entry pressure (kPa)	–	0.9	1.5	–
Pore size distribution index	3.5	–	–	–

[a] Determined using constant head permeameter [66]

[b] www.baschem.co.uk (silicone oil–water system)

[c] www.machinerylubrication.com

of PTs, one time domain reflectometry (TDR) probe (CS640) (Campbell Scientific Ltd, Shepshed, UK) was used at the corresponding position on the wall of the cell. The TDR probe (CS640) with rod length 7.5 cm and diameter 0.159 cm, was used to determine the water content of the porous medium sample locally.

Calibration of the PTs was done with a portable pressure calibrator, DPI 610 (Druck Limited, Leicester, UK) as discussed by Abidoye and Das [57]. Using the outflow weight

of water obtained on weighing balance, average domain saturation was determined using a graduated glass cylinder placed on an accurate weighing balance which was connected to the computer and data logged in real time by the weighing balance software (A&D Company Limited, San Jose, USA). This method was adopted to determine average domain scale saturation as it represents the true saturation in the domain at any particular time from a material balance point of view.

The arrangement of the column was a sort of pressure cell. At the start of a flow experiments, a predetermined amount of water was poured into the cell to a certain position. This was followed by pouring of sand using a metal sieve of appropriate size to ensure uniform sand deposition and prevent air trap while simultaneously vibrating the cell. When this was complete, excess water was drained through the outflow valve. This gave the estimate of the amount of water in the domain. At the top of the sand level, the hydrophobic filter was then placed. This prevents water flow from the top of the domain boundary. The column was then sealed with a metal cap with tubing connected to the silicone oil reservoir.

2.3 Dynamic drainage experiment

Constant pressure was maintained on the hydrophobic membrane, using an air compressor (R.E.P. Air Services, Loughborough, UK). Set pressure, regulated by a choke valve and monitored on pressure gauge was directly imposed on a column of silicone oil in a Mariotte bottle (see Fig. 2). The outflow (displaced water) was collected in a beaker placed on an accurate weighing balance. The beaker was open to the atmosphere.

For the dynamic drainage, a set pressure of either 10 or 20 kPa was imposed on the oil which pushed it to the top of the domain. When the outflow valve was opened, drainage of the porous domain began. P_c–S_w profiles were conspicuously different under different boundary conditions. Replicate runs of some of the experiments were conducted to check repeatability of the experiments. The ambient laboratory temperature was approximately 20 °C.

2.4 Methods of averaging and parameters calculation

To upscale the local values of measured quantities to the domain level, appropriate averaging technique is needed. This applies to the local pressures of both phases in order to determine capillary pressure for the entire domain at specific wetting phase saturation. The mathematical technique for the averaging is expressed below:

$$P_c^{domain}\big|_{t_n} = \left(\frac{\sum_{j=1}^{m} (1 - S_{wj})(P_{nwj})}{\sum_{j=1}^{m} (1 - S_{wj})} - \frac{\sum_{j=1}^{m} S_{wj}(P_{wj})}{\sum_{j=1}^{m} S_{wj}} \right)\Bigg|_{t_n} \tag{2}$$

where $P_c^{domain}\big|_{t_n}$ represents the domain representative capillary pressure at a particular saturation and the corresponding experimental time, t_n(s) referring to the time at nth count of data generated, P_{nw} and P_w (Pa) are the non-wetting and wetting phase pressures at the nth count of the generated data. S_w (–) refers to the wetting phase saturation and j = 1, 2, m, with m being the total number of measurement levels in the domain i.e. 2 for 8 cm and 3 for 12 cm cells.

A central difference method was applied to determine the desaturation rate ($\partial S_w/\partial t$) in the two-phase system. This was performed using the mathematical relation in Eq. (3). The method is commonly applied in related literature [6, 16]. For the local scale $\partial S_w/\partial t$, saturation data were obtained from the local TDR readings while at the domain scale, the saturation data determined from the outflow volume collected in the cylinder were used:

$$\left.\frac{\partial S_w}{\partial t}\right|_{tn} = \frac{S_w|_{t\,n+1} - S_w|_{t\,n+1}}{t_{n+1} - t_{n-1}} \tag{3}$$

2.5 Relative permeability calculation

This paper estimates the K_r–S_w relationship for entire saturation range as follows. P_c–S_w model given by van Genuchten [58] combined with Mualem's [28] model yields the following relative permeability function:

$$K_{rw} = S_w^{eff}\left[1 - \left(1 - S_w^{eff\left(\frac{1}{m}\right)}\right)^m\right]^2 \tag{4}$$

$$K_{rnw} = (1 - S_{w^{eff}})^{\frac{1}{2}}\left(1 - S_{w^{eff}}^{\left(\frac{1}{m}\right)}\right)^{2m} \tag{5}$$

where K_{rw} and K_{rnw} (–) are the relative permeability of wetting and non-wetting phase respectively, m (–) is a parameter which is related to van Genuchten pore size distribution coefficient (n), and S_w^{eff} (–) is the effective water saturation given by $\left(S_w^{eff} = (S_w - S_{rw})/(1 - S_{rw})\right)$ wherein S_{rw} (–) is residual water saturation, and S_w (–) is water saturation. For the purpose of this work, effective saturation was calculated from the experimentally measured saturation values. Then n and m were determined using the fitted van Genuchten [58] model. Using these values of effective saturation, n and m, values of K_{rw} and K_{rnw} were determined. We appreciate that van Genuchten–Mualem equations are derived under specific assumptions [28, 58]. We accept these assumptions and assume that they can be applied to the system under consideration in this work. While calculating the above parameters it was evident that the experimental data fitted well to the van Genuchten–Mualem equations.

2.6 Dynamic coefficient (τ) calculation

This work is primarily concerned with elucidating the trends in K_r–S_w. However, a brief explanation of the τ determination is included for completeness of the discussion. Furthermore this will throw light at the approach employed in this work [57]. Different approaches have been reported in the literature for this purpose. For example, the τ calculation approach of Bottero et al. [59], and Das and Mirzaei [44] differs from the approach of Camps-Roach et al. [7] and Goel and O'Carroll [3]. In this work, a similar approach to that of the Bottero et al. [59] was employed. In this approach the dynamic coefficients were calculated from the P_c–S_w data obtained for different viscosity ratios and domain scales using Eq. (1). To achieve this, the phase pressures for the non-wetting phase (P_{nw}) and the wetting phase (P_w) were interpolated, for both equilibrium and dynamic drainage conditions at selected saturations. The corresponding points for the parameters in Eq. (1) i.e. P_{nw} and P_w at a particular wetting phase saturation, S_w, were obtained for both

the dynamic and equilibrium drainage experiments. For the dynamic drainage experiments, the difference in the wetting and non-wetting phase pressures at the same saturation gives P_c^{dyn} in Eq. (1). Similarly, for the quasi static drainage experiment, the difference between the phase pressures gives P_c^{static} at the same wetting phase saturation. The saturation values were selected to cover the entire saturation range of the experiment, i.e., 0 to 1. Similarly, data for the rate of change of saturation ($\partial S_w/\partial t$) were interpolated. The plots of the differences between the dynamic and equilibrium capillary pressures ($P_c^{dyn} - P_c^{static}$) against the desaturation rates ($\partial S_w/\partial t$) at the respective water saturation for different imposed conditions were fitted with a straight line. The slope of this line gives the dynamic coefficient, τ.

At every measurement location in the domain, the respective phase pressures measured from the pressure sensors attached to that location were used in the P_c calculation for that location while S_w was also determined from the TDR reading at the location. For the domain level calculation, average P_c determined from Eq. (2) was used while the domain saturation was determined from water outflow reading on the electronic weighing balance. Most papers in the literature have used similar linear interpolation to determine the dynamic pressure difference at a specific saturation (e.g., [59].

3 Results and discussions

This paper is focussed on finding the influence of different factors which affect the K_r–S_w relationship under dynamic conditions. The work presented here is focussed especially on the effect of fluid viscosity and scale dependency for the two phase flow involving silicone oil and water for homogeneous porous domain.

3.1 P_c–S_w and $\partial S_w/\partial t - S_w$ relationships for different domain scales

To understand the behaviour of the system, we show the behaviour of the P_c–S_w curves and desaturation rate ($\partial S_w/\partial t$) under dynamic conditions at 10 kPa boundary pressure with 200 cSt silicone oil as the non-wetting phase (Fig. 3). It will be recalled that the 12 cm-high cell has three measurement points labelled as top, middle and bottom where all points are equally spaced around the domain geometry. Similarly, 8 cm-high cell has two measurement points labelled as top and bottom.

Figure 3 shows that the P_c–S_w curves are fairly similar at different depths of the domains except at the top of the domain of 12 cm high cell where the P_c–S_w profiles which is higher than at the other lower positions of the domain. Noticeable from the figure is that the final measured saturations obtained at different measurement points differ. Combinations of factors might be responsible for this. It could be attributed to the effect of pressure gradient across the height of the domain. As the distance from the injection point increases, influence of pressure drop increases. This seems to manifests in the decrease in $\partial S_w/\partial t$ values (absolute value) with increasing distance from the injection point (i.e. the lower the measurement point, the the lower the $\partial S_w/\partial t$). This also leads to the P_c–S_w relationships terminating at different saturation points at different depths of each domain. While the P_c–S_w curves at the top of each domain attain lower final measured saturation, the profile at further depths away from the injection points terminate at higher final measured saturation values. This behaviour is shown in Fig. 3a and b for 12 and 8 cm high cells, respectively. The impact of pressure gradient becomes more conspicuous in $\partial S_w/\partial t$ at different depths of

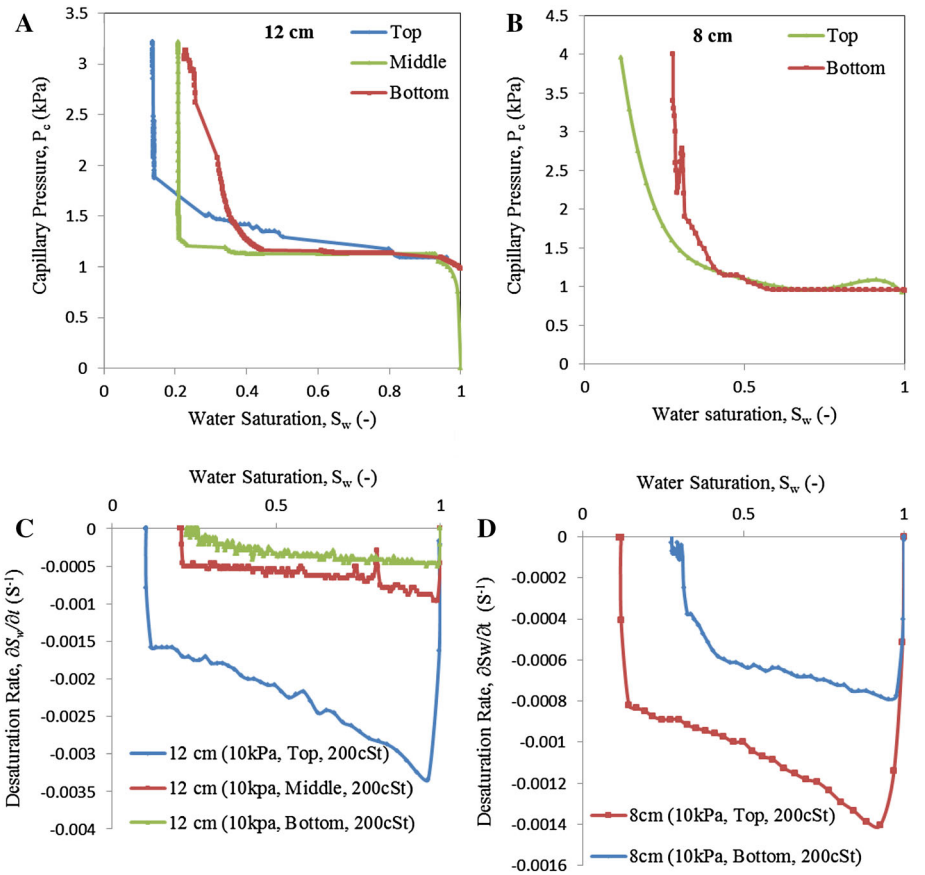

Fig. 3 P_c–S_w and $\partial S_w/\partial t$ – S_w patterns in the 8 and 12 cm high domains with 200 cSt silicone oil at 10 kPa boundary pressure

each domain as shown in Fig. 3c, d for the 12 and 8 cm high cells, respectively. Wide gap exists between the $\partial S_w/\partial t - S_w$ profile at the top of the domain compare to the other lower measurement points. In the 12 cm high cell, this trend continues at lower measurement points with $\partial S_w/\partial t - S_w$ curve remaining higher at the middle measurement positions than at the bottom position.

Also, the high viscosity of the silicone oil used in the work may be a contributing factor. However, the gap between the $\partial S_w/\partial t - S_w$ profiles at lower measurement positions (middle and bottom) is much lower compare to the gap existing between the $\partial S_w/\partial t - S_w$ profiles at the top of the domain and the middle measurement position. [59] earlier showed that the difference in P_c–S_w profiles at different averaging windows remains quite small while the difference in $\partial S_w/\partial t - S_w$ profiles at the different averaging windows appear considerable. This had been seen as the major contribution to the magnitude of the upscaled dynamic coefficient (τ). Hence, τ increases as the size of domain scale or averaging window increases [8, 59].

Similar behaviour was encountered in the P_c–S_w and $\partial S_w/\partial t - S_w$ profiles for the two-phase system with 1000 cSt silicone oil as the non-wetting phase. However, the aim of this

work is to show the effects of fluid properties, domain scale and the dynamic flow conditions on the relative permeability.

4 Effects of viscosity ratio on relative permeability–saturation relationship

To determine the effects of viscosity ratio, experiments were performed using water and silicone oil with two differing viscosities (200 and 1000 cSt respectively). It corresponds to viscosity ratio of 200 and 1000 respectively if viscosity of water is taken as 1 cSt. The results are shown in Fig. 4.

It can be easily noticed that irrespective of the fluid pair, relative permeability of the fluid increases with the increasing saturation of the respective fluid. This trend conforms to the previous literature studies. Further it can be observed that water relative permeability decreases with increasing viscosity ratio while oil relative permeability increases with increasing viscosity ratio which is in line with experimental, numerical and modeling studies [31, 41, 60]. This behaviour can be explained using lubrication effect [32, 35, 39]. As the oil displaces water (drainage), a layer of water is trapped between oil and walls of the capillary. This layer of water acts as lubricant to the movement of oil. The oil moves through the larger capillaries and the smaller capillaries filled with water are bypassed. At higher viscosity ratio water flows in the form of bubbles which results in lower relative permeability for water. The minimum residual water contents for 200 and 1000 cSt silicone oil–water were 11 and 19 %, respectively. Therefore, more water remains as residual for higher viscosity ratio. This was also observed by others [38, 61].

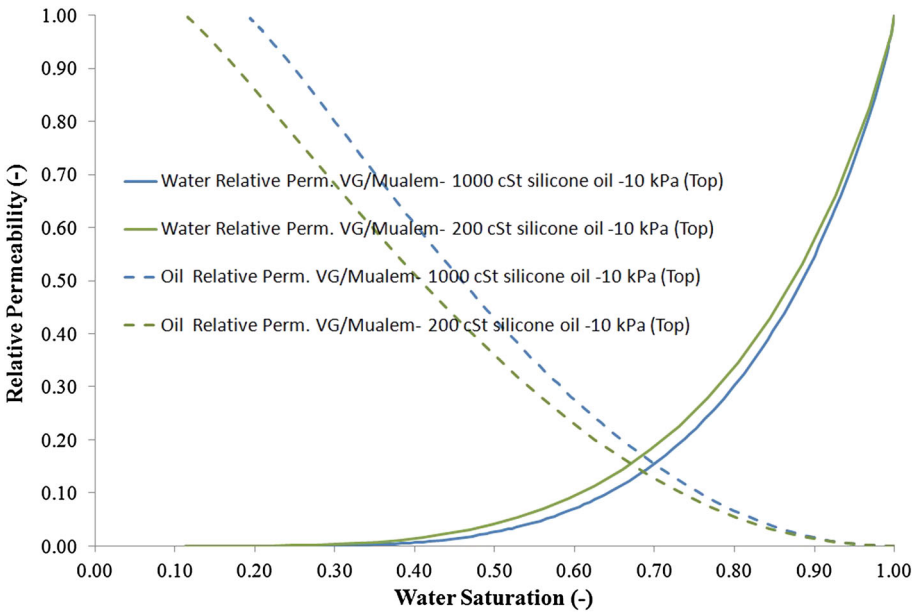

Fig. 4 Relative permeability-water saturation curves for water and silicone oil with two different viscosities (200 and 1000 cSt respectively) for 8 cm high domain and boundary pressure of 10 kPa

The maximum capillary numbers for 200 cSt and 1000 cSt oil (for 10 kPa boundary pressure and 8 cm domain) were 6.57×10^{-5} and 1.56×10^{-5}, respectively. It can be understood that water relative permeability increases whereas oil relative permeability decreases with increasing capillary number. This trend was confirmed by another research [60].

4.1 Effects of boundary pressure on dynamic relative permeability–saturation relationship

Some of the typical results are plotted in Fig. 5 for water and silicone oil (200 cSt) in 12 cm domain. It can be observed that with increasing boundary pressure water relative permeability decreases while oil relative permeability increases. This can be explained by the relative speed of flow under the different injection pressures. At the 10 kPa injection pressure, the invading oil penetrates more slowly and the water phase that wets the sand surface gets gently displaced. As the injection pressure increases to 20 kPa, the oil invades at faster speed while the response of the wetting phase may be described as sluggish owing its wettability characteristics. Also, at the 10 kPa, the pressure in the water decreases and reaches static state gradually while that of the oil increases gradually. As the injection pressure increases (20 kPa) the oil pressure rises fast while the water pressure decreases faster than before. This manifests in the K_{rnw} becoming higher with pressure and K_{rw} becoming lesser with pressure.

Earlier research by Ataie-Ashtiani et al. [62] showed that pressure gradient could significantly influence K_r–S_w relationship. In comparisons, Gao et al. [30] showed that the relative permeability increased with increasing injection for both wetting and non-wetting

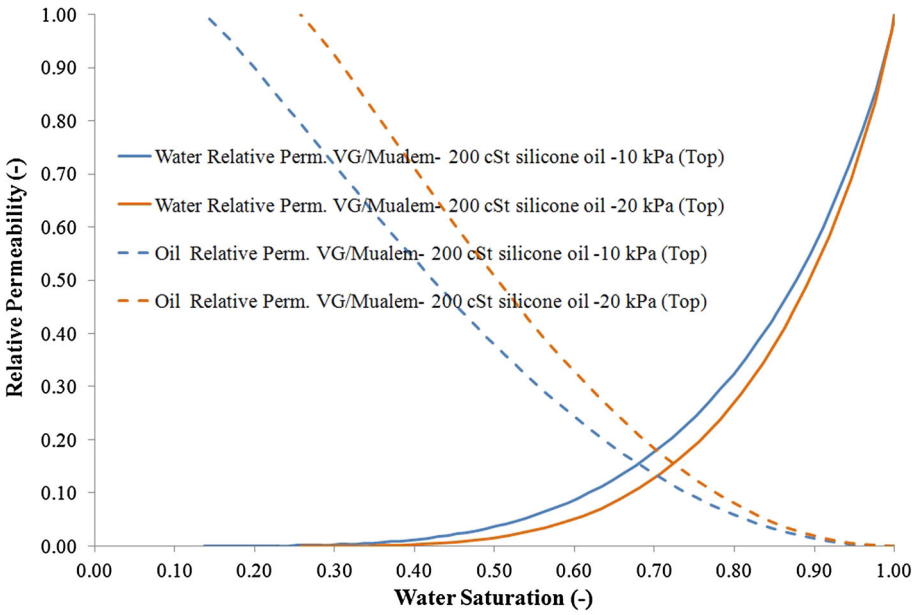

Fig. 5 Relative permeability-water saturation curves for water and silicone oil (200 cSt) for 12 cm high domain and boundary pressures of 10 and 20 kPa

phases and observed inconsistencies in this trend. However, both of these [30, 62] were modeling studies on heterogeneous systems. Gawish and Al-Homadhi [63] earlier found that the oil relative permeability decreased with increasing boundary pressure. Their investigations were conducted under steady state unlike the dynamic condition in the present study. So, it can be inferred that the relative permeability of the non-wetting phase generally increases with boundary pressure, while the trend in the wetting phase cannot be conclusively inferred. Although the results presented in this section are for silicone oil of viscosity 200 cSt, the same general conclusion can be made for oil of other properties, namely, silicone oil of viscosity 1000 cSt.

The maximum capillary number for 10 and 20 kPa boundary pressure (for 200 cSt oil and 12 cm domain) were found to be 5.68×10^{-5} and 1.79×10^{-4} respectively. It suggests that the oil relative permeability increases whereas the water relative permeability decreases with increase in the capillary number.

4.2 Effects of domain size on dynamic relative permeability–saturation relationship

The results are plotted in Fig. 6 for water and silicone oil (200 cSt) in 8 and 12 cm domain. Domain scale average values are used for plotting Fig. 6. Averaging is done as per the standard procedure given above. The values K_{rnw} obtained at the scales of 8 cm and 12 cm are almost similar while K_{rnw} values differ slightly at the low water saturation values. The similarity in these curves was expected as the permeability is the same. The difference in non-wetting phase relative permeability at low water saturation may be due to the presence of micro scale heterogeneities [42, 44, 62].

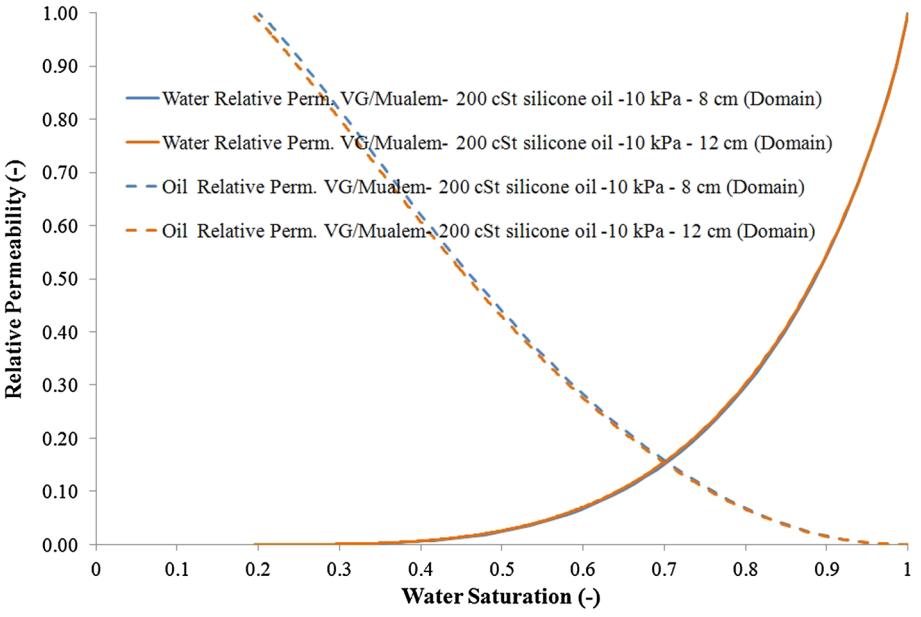

Fig. 6 Relative permeability-water saturation curves for water and silicone oil (200 cSt) for boundary pressure of 10 kPa in 8 and 12 cm domains

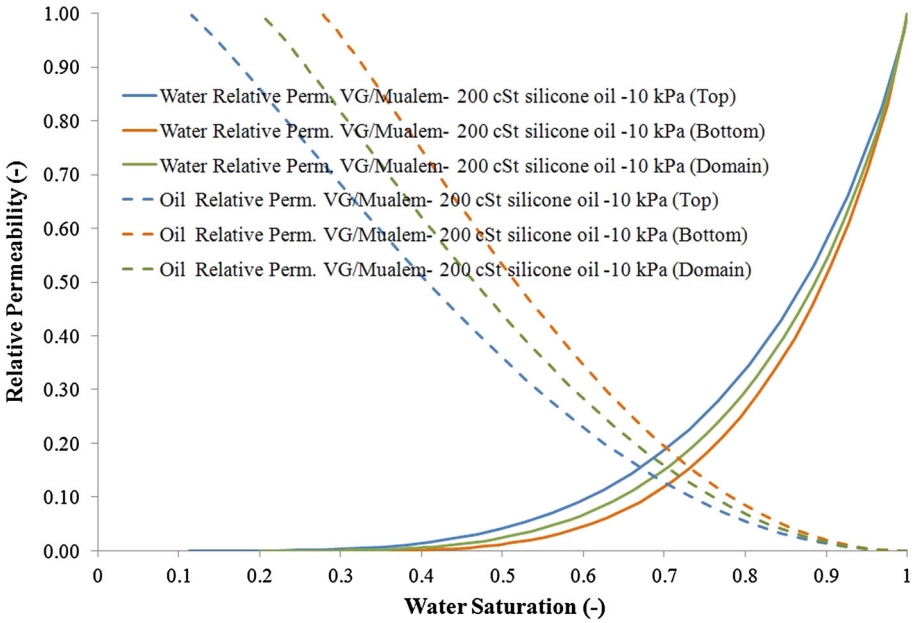

Fig. 7 Relative permeability-water saturation curves for water and silicone oil (200 cSt) for boundary pressure of 10 kPa in 8 cm high domain

4.3 Effects of location on relative permeability–saturation relationship

The results are plotted in Fig. 7 for water and silicone oil (200 cSt) in 8 cm domain. It can be observed that at the top of the column relative permeability of water is higher than that of the bottom if the saturation is uniform throughout the column. This trend is opposite for the oil relative permeability. But in reality because of the saturation gradients water relative permeability is less at the top and more at the bottom. An average of the top and bottom relative permeability is also plotted which lies in between of the top and bottom relative permeability.

4.4 Comparison of static and dynamic relative permeability–saturation relationships

The results are plotted in Fig. 8 for water and silicone oil (1000 cSt) in 12 cm domain. It can be observed that at the top of the column dynamic relative permeability of water is higher than that of the static relative permeability of water. This trend is opposite for the oil relative permeability. Similar results were obtained at other levels and in other domain size (8 cm). These results are qualitatively similar as obtained in previous experimental and modeling studies [64, 65]. In previous studies this behaviour was linked at low capillary numbers (Ca).

5 Mobility ratio (m) and dynamic coefficient (τ)

In order to quantify effects of the stability of fluid fronts, mobility ratio (m) [2] was computed using Eq. (6) and the results are plotted to include comparison with dynamic coefficient (Figs. 8, 9).

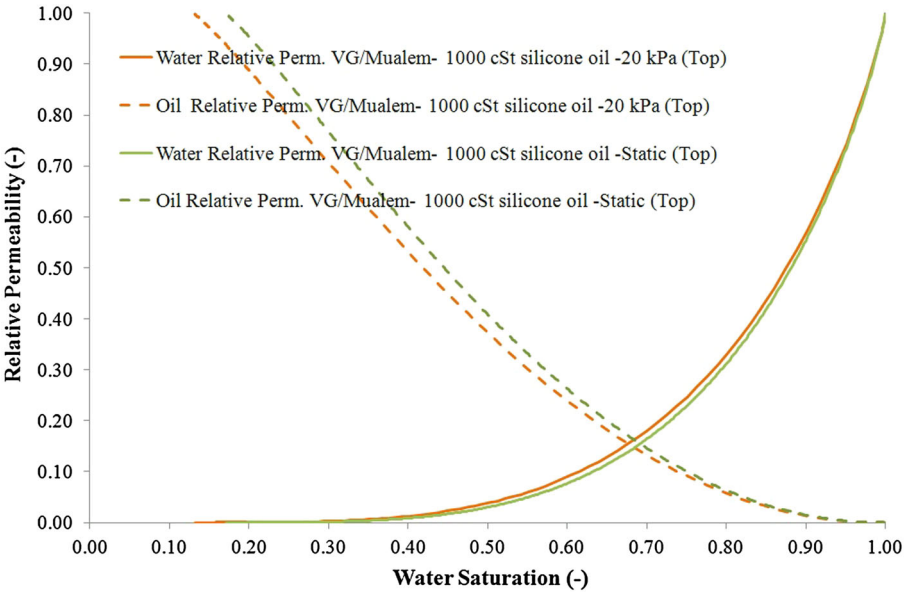

Fig. 8 Comparison of static and dynamic relative permeability versus water saturation curves for water and silicone oil (1000 cSt) for 12 cm high domain

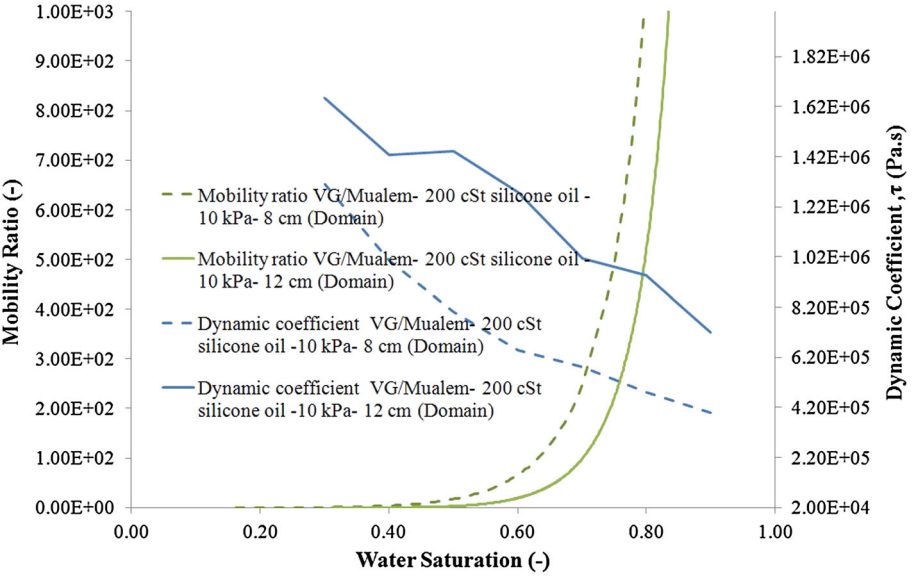

Fig. 9 Plots of mobility ratio (m) and dynamic coefficient (τ) as a function of water saturation with 200 cSt silicone oil at the top boundary pressure of 10 kPa for 8 and 12 cm high domains

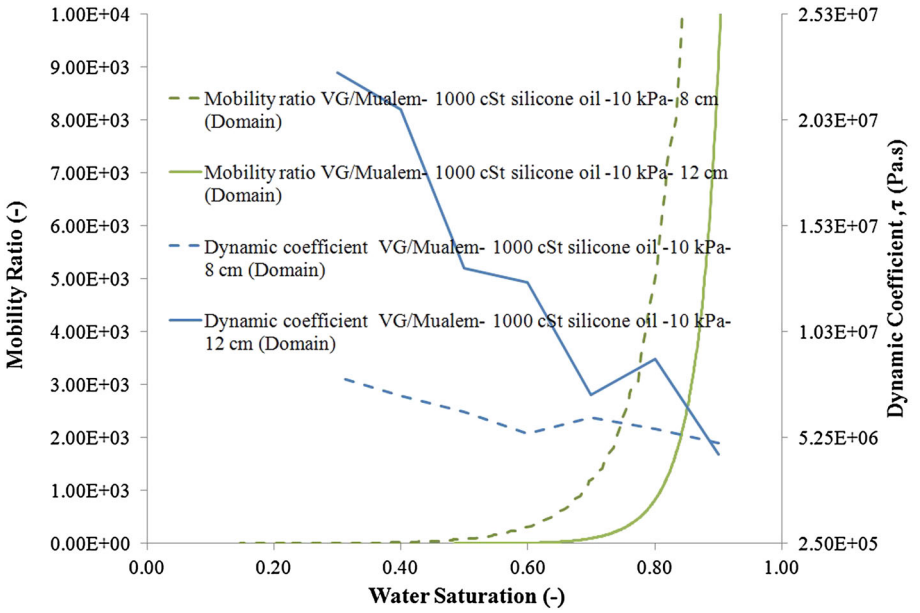

Fig. 10 Plots of mobility ratio (m) and dynamic coefficient (τ) as a function of water saturation with 1000 cSt silicone oil at the boundary pressure of 10 kPa for 8 and 12 cm high domains

$$m = \left(\frac{K_{rw}\,\mu^{n}}{K_{rnw}\,\mu^{w}}\right) \tag{6}$$

For 200 cSt oil (Fig. 9) it was observed that the mobility ratio decreased with increase in domain size while the dynamic coefficient was found to be increasing. Similar trend was noticed in 1000 cSt oil (Fig. 10). Since for a saturation of 50 %, the value of mobility ratio is more than 1, the fluid fronts are considered to be stable. The trend observed here are similar to as observed by [2, 13], i.e., as m decreases τ increases at a given saturation.

6 Conclusions

Experiments under dynamic conditions were conducted using silicone oil and water. K_r–S_w relationship is susceptible to the influence of fluid properties (i.e. viscosity) and porous media characteristics. In this study the focus has been to investigate the influence of fluid viscosity together with the role of domain scale on dynamic relative permeability-saturation (K_r–S_w) relationship in addition to the boundary condition effect. K_{rw} increases with increasing wetting phase saturation and decreases with the increase in viscosity ratio. On the other hand, K_{rnw} increases with increasing non-wetting phase saturation as well as with the increase in viscosity ratio. Also, the water relative permeability decreases while the oil relative permeability increases with the increasing boundary pressure. The boundary pressure effect is significant in comparison to fluid viscosity ratio and scale dependency. At 40 % water saturation and for 8 cm high domain, the K_{rnw} increased by 24.5 % when viscosity ratio was increased from 200 to 1000. Same is true for 12 cm high domain. The

boundary pressure, location of sensors and fluid viscosity play significant role in K_r–S_w relationship. The dynamic relative permeability curves are different from the static relative permeability curves, which is in line with previous studies. This study shows that K_r–S_w is affected by dynamic effects and therefore provisions must be made in models to include these dynamic K_r–S_w relationships. In general, the dynamic capillary pressure–saturation relationship varies depending on the location of the measurement point (e.g., top or bottom of a domain in reference to a fluid injection point). Hence, the relative permeability–saturation curves varies accordingly. The rate dependencies of these curves have not been analysed in great detail in this paper and they would need further analysis in another piece of work.

Acknowledgments This study has been carried in the framework of the EPSRC (UK) Project GR/S94315/01, ''microheterogeneity and temperature effects on dynamic capillary pressure–saturation relationships for two-phase flow in porous media.'' A PhD studentship awarded to Mr Luqman Abidoye under the Petroleum Technology Development Fund (PTDF), Nigeria, to carry out the work in this paper is much appreciated. Support from the Technical Support Team at Department of Chemical Engineering, Loughborough University, UK, for building the rig (Fig. 2) is gratefully acknowledged. We declare that there is no conflict of interests for this work. All underlying research material may be accessed by contacting the corresponding author.

References

1. Miller CT et al (1998) Multiphase flow and transport modeling in heterogeneous porous media: challenges and approaches. Adv Water Resour 21:77–120
2. Das DB, Gauldie R, Mirzaei M (2007) Dynamic effects for two-phase flow in porous media: fluid property effects. AIChE J 53(10):2505–2520
3. Goel G, O'Carroll DM (2011) Experimental investigation of nonequilibrium capillarity effects: fluid viscosity effects. Water Resour Res. doi:10.1029/2010WR009861
4. Hou L, Sleep BE, Kibbey TCG (2014) The influence of unavoidable saturation averaging on the experimental measurement of dynamic capillary effects: a numerical simulation study. Adv Water Resour 66:43–51
5. Joekar-Niasar V, Hassanizadeh SM (2011) Effect of fluids properties on non-equilibrium capillarity effects: dynamic pore-network modelling. Int J Multiphase Flow 37:198–214
6. Bottero S et al (2011) Nonequilibrium capillarity effects in two-phase flow through porous media at different scales. Water Resour Res 47(10):W10505
7. Camps-Roach G et al (2010) Experimental investigation of dynamic effects in capillary pressure: grain size dependency and upscaling. Water Resour Res 46:W08544
8. Dahle HK, Celia MA, Hassanizadeh SM (2005) Bundle-of-tubes model for calculating dynamic effects in the capillary-pressure-saturation relationship. Transp Porous Media 58(1–2):5–22
9. Mirzaei M, Das DB (2013) Experimental investigation of hysteretic dynamic effect in capillary pressure–saturation relationship for two-phase flow in porous media. AIChE J 59(10):3958–3974
10. Hanspal NS et al (2013) Artificial neural network (ANN) modeling of dynamic effects on two-phase flow in homogenous porous media. J Hydroinformatics 15(2):540–554
11. Tian S et al (2012) Dynamic effect of capillary pressure in low permeability reservoirs. Pet Explor Dev 39(3):405–411
12. Das DB, Mirzaei M, Widdows N (2006) Non-uniqueness in capillary pressure-saturation-relative permeability relationships for two-phase flow in porous media: interplay between intensity and distribution of random micro-heterogeneities. Chem Eng Sci 61(20):6786–6803
13. Hou L, Chen L, Kibbey TCG (2012) Dynamic capillary effects in a small-volume unsaturated porous medium: implications of sensor response and gas pressure gradients for understanding system dependencies. Water Resour Res 48(11):W11522

14. Mirzaei M, Das DB (2007) Dynamic effects in capillary pressure-saturations relationships for two-phase flow in 3D porous media: implications of micro-heterogeneities. Chem Eng Sci 62(7):1927–1947
15. Hassanizadeh SM, Celia MA, Dahle HK (2002) Dynamic effect in the capillary pressure-saturation relationship and its impacts on unsaturated flow. Vadose Zone J 1(1):38–57
16. Das DB, Mirzaei M (2012) Dynamic effects in capillary pressure relationships for two-phase flow in porous media: experiments and numerical analyses. AIChE J 58(12):3891–3903
17. Diamantopoulos E, Durner W (2012) Dynamic nonequilibrium of water flow in porous media: a review. Vadose Zone J. doi:10.2136/vzj2011.0197
18. Kalaydjian FJ-M (1992) Dynamic capillary pressure curve for water/oil displacement in porous media: theory vs. experiment. In: 67th SPE annual technical conference and exhibition. Society of Petroleum Engineers Inc, Washington, DC
19. O'Carroll DM et al (2005) Prediction of two-phase capillary pressure-saturation relationships in fractional wettability systems. J Contam Hydrol 77(4):247–270
20. O'Carroll DM, Phelan TJ, Abriola LM (2005) Exploring dynamic effects in capillary pressure in multistep outflow experiments. Water Resour Res. doi:10.1029/2005WR004010
21. Oung O, Hassanizadeh SM, Bezuijen A (2005) Two phase flow experiments in a geocentrifuge and the significance of dynamic capillary pressure. J Porous Media 8(3):247–257
22. Sakaki T, O'Carroll DM, Illangasekare TH (2010) Dynamic effects in field soil water retention curves: direct laboratory quantification of dynamic coefficient for drainage and wetting cycles. Vadose Zone J 9:424–437
23. Stauffer F (1978) Time dependence of the relations between capillary pressure, water content and conductivity during drainage of porous media. In: IAHR symposium on scale effects in porous media, Thessaloniki, Greece
24. Wildenschild D, Hopmans JW, Simunek J (2001) Flow rate dependence of soil hydraulic characteristics. Soil Sci Soc Am J 65(1):35–48
25. Zhang H et al (2014) Investigation of dynamic effect of capillary pressure in ultra-low permeability sandstones. Indian Geotech J 45:1–10
26. Hassanizadeh SM, Gray WG (1993) Toward an improved description of the physics of 2-phase flow. Adv Water Resour 16(1):53–67
27. Burdine NT (1953) Relative permeability calculations from pores sizes distribution data. Pet Trans 198:71–78
28. Mualem Y (1976) A new model for predicting the hydraulic conductivity of unsaturated porous media. Water Resour Res 12(3):513–522
29. Gerhard JI, Kueper BH (2003) Relative permeability characteristics necessary for simulating DNAPL infiltration, redistribution, and immobilization in saturated porous media. Water Resour Res 39(8):SBH 7-1–SBH 7-17
30. Gao S, Meegoda J, Hu L (2013) Simulation of dynamic two-phase flow during multistep air sparging. Transp Porous Media 96(1):173–192
31. Ahmadlouydarab M, Liu Z-SS, Feng JJ (2012) Relative permeability for two-phase flow through corrugated tubes as model porous media. Int J Multiph Flow 47:85–93
32. Amaefule JO, Handy LL (1982) The effect of interfacial tensions on relative oil/water permeabilities of consolidated porous media. Soc Pet Eng J 22:371–381
33. Avraam DG, Payatakes AC (1995) Flow regimes and relative permeabilities during steady-state two-phase flow in porous media. J Fluid Mech 293:207–236
34. Demond AH, Roberts PV (1987) An examination of relative permeability relations for two-phase flow in porous media. Water Resour Bull 23:617–628
35. Dou Z, Zhou ZF (2013) Numerical study of non-uniqueness of the factors influencing relative permeability in heterogeneous porous media by lattice Boltzmann method. Int J Heat Fluid Flow 42:23–32
36. Downie J, Crane FE (1961) Effect of viscosity on relative permeability. Soc Pet Eng J. 1:59–60
37. Leverett MC (1939) Flow of oil/water mixtures through unconsolidated sands. Trans AIME 132:149
38. Nejad K, Berg E, Ringen J (2011) Effect of oil viscosity on water/oil relative permeability. In: International symposium of the society of core analysts, Austin, TX, USA
39. Odeh AS (1959) Effect of viscosity ratio on relative permeability. Trans AIME 216:346–353
40. Wang J, Dong M, Asghari K (2006) Effect of oil viscosity on heavy oil–water relative permeability curves. In: SPE/DOE symposium on improved oil recovery, Society of Petroleum Engineers, Tulsa, Oklahoma, USA
41. Yiotis AG et al (2007) A lattice boltzmann study of viscous coupling effects in immiscible two-phase flow in porous media. Colloids Surf A 300:35–49
42. Das DB et al (2004) A numerical study of micro-heterogeneity effects on upscaled properties of two-phase flow in porous media. Transp Porous Media 56(3):329–350

43. Petersen RT, Balhoff MT, Bryant S (2011) Coupling multiphase pore-scale models to account for boundary conditions: application to 2D quasi-static pore networks. J Multiscale Model 03(03):109–131
44. Das DB, Mirzaei M (2013) Experimental measurement of dynamic effect in capillary pressure relationship for two-phase flow in weakly layered porous media. AIChE J 59(5):1723–1734
45. DiCarlo DA (2004) Experimental measurements of saturation overshoot on infiltration. Water Resour Res 40(4):W04215
46. van Duijn CJ, Floris FJT (1992) Mathematical analysis of the influence of power-law fluid rheology on a capillary diffusion zone. J Pet Sci Eng 7(3–4):215–237
47. van Duijn CJ et al (2013) Travelling wave solutions for degenerate pseudo-parabolic equations modelling two-phase flow in porous media. Nonlinear Anal 14(3):1361–1383
48. Rohde C, Kissling F (2010) The computation of nonclassical shock waves with a heterogeneous multiscale method. Netwo Heterog Media 5(3):661–674
49. Kissling F, Helmig R, Rohde C (2012) Simulation of infiltration processes in the unsaturated zone using a multiscale approach. Vadose Zone Journal. doi:10.2136/vzj2012.0105
50. DiCarlo DA (2013) Stability of gravity-driven multiphase flow in porous media: 40 Years of advancements. Water Resour Res 49(8):4531–4544
51. Barker JW, Thibeau S (1997) A Critical Review of the Use of Pseudorelative Permeabilities for Upscaling. SPE Reservoir Engineering (Society of Petroleum Engineers) 12(2):138–143
52. Gasda SE, Celia MA (2005) Upscaling relative permeabilities in a structured porous medium. Adv Water Resour 28(5):493–506
53. Nick HM, Matthäi SK (2011) Comparison of three FE-fv numerical schemes for single- and two-phase flow simulation of fractured porous media. Transp Porous Media 90(2):421–444
54. Renard P, De Marsily G (1997) Calculating equivalent permeability: a review. Adv Water Resour 20(5–6):253–278
55. Sharifi M, Kelkar M (2013) New dynamic permeability upscaling method for flow simulation under depletion drive and no-crossflow conditions. Pet Sci 10(2):233–241
56. Yang Z et al (2012) Upscaling of the constitutive relationships for CO_2 migration in multimodal heterogeneous formations. Int J Greenhouse Gas Control 19:743–755
57. Abidoye LK, Das DB (2014) Scale dependent dynamic capillary pressure effect for two-phase flow in porous media. Adv Water Resour 74:212–230
58. van Genuchten MT (1980) A closed form equation for predicting the hydraulic conductivity of unsaturated soils. Soil Sci Soc Am J 44:892–898
59. Bottero S, Hassanizadeh SM, Kleingeld PJ (2011) From local measurements to an upscaled capillary pressure–saturation curve. Transp Porous Media 88(2):271–291
60. Mohanty KK (2002) Impact of capillary and bond numbers on relative permeability. University of Houston, Houston, p 119
61. Abrams, A., (1975),The influence of fluid viscosity, interfacial tension, and flow velocity on residual oil saturation left by waterflood. SPE 5050
62. Ataie-Ashtiani B, Hassanizadeh SM, Celia MA (2002) Effects of heterogeneities on capillary pressure-saturation-relative permeability relationships. J Contam Hydrol 56(3–4):175–192
63. Gawish A, Al-Homadhi E (2008) Relative permeability curves for high pressure, high temperature reservoir conditions. Oil Gas Bus 2
64. Joekar-Niasar V, Hassanizadeh SM (2011) Specific interfacial area: the missing state variable in two-phase flow equations? Water Resour Res 47(5):W05513
65. Tsakiroglou CD, Avraam DG, Payatakes AC (2007) Transient and steady-state relative permeabilities from two-phase flow experiments in planar pore networks. Adv Water Resour 30(9):1981–1992
66. Bear J (2013) Dynamics of fluids in porous media. Dover Publications, Mineola